THE ULTRA WEAK VARIATIONAL FORMULATION FOR ELASTIC WAVE PROBLEMS[¶]

T. HUTTUNEN[*‡], P. MONK[†], F. COLLINO[§], AND J.P. KAIPIO[*]

Abstract. The ultra weak variational formulation has been used effectively to solve time-harmonic acoustic and electromagnetic wave propagation in inhomogeneous media. We develop the ultra weak variational formulation for elastic wave propagation in two space dimensions. In order to improve the accuracy and stability of the method we find it necessary to approximate the S- and P- wave components of the solution in a balanced way. Some preliminary analysis is provided and numerical evidence is presented for the efficiency of the scheme in comparison to piecewise linear finite elements.

Key words. elastic waves, scattering, ultra weak variational formulation, finite element method

AMS subject classifications. 74J05 74J20 74S30

1. Introduction. When modeling the propagation of time-harmonic ultrasonic waves through human bone we are faced with the problem of solving the equations of time-harmonic elastic wave propagation in a medium with complicated shape and potentially spatially varying parameters (see for example [15] and [23]). Furthermore the wavelength of the acoustic field can be small in comparison to the size of anatomical structures (a typical wavelength in our application is 2-6 mm) so that a method suitable for higher frequencies is needed.

Of course there is no shortage of methods for this important problem which arises in other areas of applications including seismic wave propagation (see for example [8]) and non-destructive testing (see for example [1]). Given the complicated geometry of the problem and the need to allow spatially varying elastic parameters an obvious candidate is the finite element method (see for example [7] for the standard approach to elastostatics and [11] for an improved scheme for the time-harmonic problem). In order to resolve a wave, the finite element grid needs to be sufficiently fine compared to the wavelength of the elastic wave. Typically, for a piecewise linear scheme, at least 10 grid points per wavelength are needed to resolve the wave, and even more if wave propagation is to be accurately modeled over many wavelengths [18]. Of particular relevance to the elastic wave equation is that the wavelength used to estimate the mesh size based on fixing the number of points per wavelength must be the shortest appearing in the computation (the wavelength of the S-wave). Higher order schemes can help with this problem by decreasing the number of grid points per wavelength needed to attain a given accuracy (see Section 4.7 of [18]). A final, and not inconsequential, point is that the finite element method results in a linear system that is not easy to solve by standard fast methods such as multigrid. This is because the finite element matrix is indefinite (at least for a sufficiently short wavelength compared to the size of the computational domain).

Given the difficulties outlined above for the finite element method for this prob-

[*]Department of Applied Physics, University of Kuopio, P.O.Box 1627, 70200 Kuopio, Finland

[†]Department of Mathematical Sciences, University of Delaware, Newark, DE 19711, USA

[‡]Brigham & Women's Hospital, Harvard Medical School, 221 Longwood Avenue, Boston, MA 02115, USA

[§]CERFACS, 42 Avenue G. Coriolis, 31057 Toulouse cedex, France

[¶]This work was supported by the Finnish Academy Grant 72431. The research of PM was supported in part by grant number F49620-02-01-0071 from the US AFOSR.

lem, it is natural to ask if other finite element type procedures can be developed which have the flexibility of the finite element scheme, but improved properties when applied to the elastic wave propagation problem. In this paper we shall develop an application of the Ultra Weak Variational Formulation (UWVF) to the time-harmonic elastic wave equation. This method was developed by Cessenat and Després [5, 6] for the Helmholtz equation and by Cessenat [4, 6] for Maxwell's equations, and we follow their nomenclature. In particular the method is based on a variational principle. Since finite element methods that use continuous elements are often said to be based on a "weak" form of the differential equation, this method is said to be "ultra weak" since it uses discontinuous elements. Our positive experience with this scheme in both these applications shows that the UWVF has several attractive features. It is based on a finite element decomposition of space and hence is able to approximate geometric features as well as the finite element method. However, instead of using piecewise polynomials to discretize the problem, the UWVF uses plane wave solutions of the underlying wave equation on each element (hence the basis is globally discontinuous). By varying the number of these solutions used on each element the effective order of convergence of the method can be changed, and the conditioning of the problem controlled to some extent (see [13]). The matrix equation resulting from the UWVF is also simpler to solve than the finite element matrix problem and in our experience a bi-conjugate gradient method can provide an accurate solution (of course this method does not approach multigrid efficiencies but does allow the solution of problems without the need for factoring the matrix).

Of course the UWVF is not a panacea and even its originators note that it is rather complex [5]. The UWVF method does not directly provide an approximation to the field at all points in space unless the solution is post-processed. However the displacement field and traction can be recovered on faces of the mesh without difficulty. Only piecewise constant elastic coefficients can be handled (due to the need for explicit solutions of the underlying equations), but rather general transmission conditions across internal interfaces are easy to incorporate. The conditioning of the linear system is sensitive to the correct choice of the approximating functions on each element. If too many functions are used, the conditioning deteriorates. For this reason we have advocated choosing the basis dynamically during the assembly of the relevant matrices [13]. Finally the UWVF does not avoid the need for a sufficiently fine discretization compared to the wavelength of the sound. However, we shall see that the S-wave and P-wave components of the displacement can be approximated independently in the UWVF. Furthermore, by using larger elements and larger numbers of plane waves per element the density of unknowns can be reduced below that needed for a low order finite element scheme.

This paper will be devoted to developing the UWVF for the linear time-harmonic equations of elasticity in two dimensions. In the future we will extend the study to three dimensions and the fluid structures interaction problem. In the next section we define the problem to be studied and discuss appropriate boundary conditions. The UWVF is developed in Section 3 and discretized in Section 4. This development requires two ingredients. First and most critical, initial attempts to develop an UWVF for the elasticity problem suffered from very poor conditioning of the resulting matrix problem. In our early work we used the same number of basis functions to approximate both the S- and P-waves. In this paper the conditioning problem is reduced by using a basis that approximates the S- and P-waves in a balanced way. Particularly when there is a large discrepancy in the wavenumber for the S- and P-waves this is essential

to improve conditioning. Second, we require an absorbing boundary condition in order to simulate elastic scattering problems. This is provided by special absorbing boundary condition (ABC) for the elasticity problem developed in [14]. The ABC provides a low order absorbing boundary condition appropriate for these equations. It is also used to provide inter-element coupling.

The error analysis of the UWVF is not as well developed as the error analysis of the finite element method. We report results in the context of the elasticity problem in Section 5. Finally, in Section 6 we report a numerical study that shows why we need to consider approximating the S- and P-waves in a balanced way and compare the elastic UWVF to a classical piecewise linear finite element method. We also solve a problem exhibiting Rayleigh waves and a transmission problem to illustrate the method on more complex problems. These examples show that the the elastic UWVF is worthy of future study.

We should mention that this study is not the first to advocate the use of plane waves as part of an algorithm for the elasticity problem. Perrey-Debain *et al.* [21, 22] describe a partition of unity type method for an integral equation for the time-harmonic linear elastic wave problem. Their method shows considerable promise but is aimed at solving for the field in a homogeneous isotropic medium with standard boundary conditions whereas the UWVF can handle inhomogeneous material coefficients and mixed boundary conditions. An alternative approach would be to apply the method of Babŭska and Melenk [3, 19] to the elastic wave equation. This deserves to be looked at but it seems to be more difficult to incorporate variable material properties in this formulation.

2. The time-harmonic elastic wave equation. In this section we shall define the problem to be solved paying particular attention to boundary conditions. As we discussed in the Introduction we are interested in studying two dimensional linearized time-harmonic elastic wave propagation. Consider linearized elastic wave motion in an inhomogeneous medium occupying a bounded Lipschitz polygonal domain $\Omega \subset \mathbb{R}^2$. We suppose that the elastic properties of the medium occupying Ω are piecewise constant functions of position. Thus we can write $\overline{\Omega} = \cup_{j=1}^{J} \overline{\Omega_j}$ where the overline indicates closure, and $\{\Omega_j\}_{j=1}^{J}$ is a collection of non-overlapping Lipschitz domains. On each Ω_j the Lame constants λ and μ and the density of the medium ρ are independent of position. Then the time-harmonic displacement vector $\mathbf{u}$ satisfies the Navier equation [10]

$$\mu \Delta \mathbf{u} + (\lambda + \mu) \nabla (\nabla \cdot \mathbf{u}) + \omega^2 \rho \mathbf{u} = 0 \quad \text{in } \Omega_j \tag{2.1}$$

for each Ω_j. Here ω is the angular frequency of the field. The Lamé constants can be expressed by means of the Poisson ratio ν and Young's modulus E as follows

$$\mu = \frac{E}{2(1+\nu)}, \qquad \lambda = \frac{E\nu}{(1+\nu)(1-2\nu)}.$$

In order to model dissipation we allow E to be complex valued and in particular $E = E' - iE''$, $(E',\ E'' \geq 0)$ where E' is the standard Young's modulus and E'' is often called the loss modulus and is a non-negative piecewise constant function of position. We shall assume the density and frequency are real. Although we shall formulate the UWVF for complex valued coefficients, our analysis and examples will have real valued coefficients.

To complete the description of the problem we need a boundary condition on the boundary of Ω denoted by Γ, and we need to make precise how the fields on the

different subdomains Ω_j are related across interfaces between regions with different elastic properties. Let $\mathbf{n}$ be a unit normal to a curve S. Then on S we define the traction operator $\mathbf{T}^{(\mathbf{n})}$ formally by

$$\mathbf{T}^{(\mathbf{n})}(\mathbf{u}) = 2\mu\frac{\partial \mathbf{u}}{\partial n} + \lambda \mathbf{n}\nabla\cdot\mathbf{u} + \mu\mathbf{n}\times\nabla\times\mathbf{u} \tag{2.2}$$

where the functions are evaluated on S. If the coefficients λ and μ are discontinuous at S, the choice of the coefficients in $\mathbf{T}$ depend on which side of S the traction is being evaluated. The operator $\mathbf{T}$ maps local displacements to local tractions on the boundary S.

The Navier equation is assumed to be satisfied on each subdomain Ω_j, and across subdomain boundaries continuity of the displacement $\mathbf{u}$ and the traction $\mathbf{T}$ ensures that the global function solves the elastic wave problem. In particular, suppose subdomains Ω_{j_1} and Ω_{j_2} meet at a common edge Σ_{j_1,j_2} where $\Sigma_{j_1,j_2} = \overline{\Omega}_{j_1}\cap\overline{\Omega}_{j_2}$. Suppose $\mathbf{n}_{j_\ell}$ is the unit outward normal to Ω_{j_ℓ}, $\ell = 1,2$. In Ω_{j_1} and Ω_{j_2} the Navier equation (2.1) is satisfied using the appropriate elastic coefficients and density for that domain. On the interface Σ_{j_1,j_2} the continuity of the displacement and the stress leads to transmission conditions

$$\left.\begin{array}{rcl} \mathbf{u}|_{\Omega_{j_1}} & = & \mathbf{u}|_{\Omega_{j_2}} \\ \mathbf{T}^{(\mathbf{n}_{j_1})}(\mathbf{u}|_{\Omega_{j_1}}) & = & -\mathbf{T}^{(\mathbf{n}_{j_2})}(\mathbf{u}|_{\Omega_{j_2}}) \end{array}\right\} \quad \text{on } \Sigma_{j_1,j_2}, \tag{2.3}$$

where $\mathbf{T}$ is given by (2.2) and the coefficients on Ω_{j_ℓ} are used to evaluate $\mathbf{T}^{(\mathbf{n}_{j_\ell})}(\mathbf{u}|_{\Omega_{j_\ell}})$, $\ell = 1,2$. For the UWVF these transmission conditions are combined into Robin type boundary conditions. Let σ denote a positive-definite real valued matrix function of position on Σ_{j_1,j_2} (we shall say how we choose σ in Section 2.1) and we demand that on Σ_{j_1,j_2}

$$\begin{aligned} \mathbf{T}^{(\mathbf{n}_{j_1})}(\mathbf{u}|_{\Omega_{j_1}}) + i\sigma\mathbf{u}|_{\Omega_{j_1}} &= -\mathbf{T}^{(\mathbf{n}_{j_2})}(\mathbf{u}|_{\Omega_{j_2}}) + i\sigma\mathbf{u}|_{\Omega_{j_2}}, \\ \mathbf{T}^{(\mathbf{n}_{j_1})}(\mathbf{u}|_{\Omega_{j_1}}) - i\sigma\mathbf{u}|_{\Omega_{j_1}} &= -\mathbf{T}^{(\mathbf{n}_{j_2})}(\mathbf{u}|_{\Omega_{j_2}}) - i\sigma\mathbf{u}|_{\Omega_{j_2}}. \end{aligned}$$

Obviously these transmission conditions are equivalent to the original pair.

For the boundary Γ of Ω, we use a special type of boundary condition motivated by previous work on the UWVF for the Helmholtz and Maxwell equations [4]. In particular, let Q denote a scalar function of position on Γ and let $\sigma \in \mathbb{R}^{2\times 2}$ denote a real valued and symmetric positive definite matrix function of position on Γ (both functions need to have entries in $L^\infty(\Gamma)$ and are assumed to be uniformly bounded). Suppose Γ has unit outward normal $\mathbf{n}$. The boundary condition on Γ is then written as

$$\mathbf{T}^{(\mathbf{n})}(\mathbf{u}) - i\sigma\mathbf{u} = Q(-\mathbf{T}^{(\mathbf{n})}(\mathbf{u}) - i\sigma\mathbf{u}) + \mathbf{g} \quad \text{on } \Gamma \tag{2.4}$$

where $\mathbf{g} \in (L^2(\Gamma))^2$ is a given function providing the source term. With different choices of Q and σ a variety of boundary conditions can be implemented. For example, if $Q = 1$, we obtain the traction boundary condition

$$\mathbf{T}^{(\mathbf{n})}(\mathbf{u}) = \frac{1}{2}\mathbf{g} \text{ on } \Gamma \tag{2.5}$$

whereas when $Q = -1$ we obtain the displacement boundary condition

$$\mathbf{u} = i\frac{\sigma^{-1}}{2}\mathbf{g} \text{ on } \Gamma. \tag{2.6}$$

When $Q = 0$ we obtain a Robin type boundary condition. With the choice σ given in Section 2.1 this provided a low order absorbing boundary condition for the elastic wave equation.

We shall assume that the Lamé constants, angular frequency and functions Q, σ and $\mathbf{g}$ have been chosen so that there is a unique solution $\mathbf{u} \in (H^1(\Omega))^2$ of the Navier equation (2.1) together with the transmission conditions (2.3) and the boundary condition (2.4). Further assumptions on $\mathbf{u}$ will be made as we derive the UWVF.

Since Q and σ can be functions of position the above boundary conditions (2.5) and (2.6) can be mixed on a single surface or on different surface components. Obviously we need a method for choosing σ and we consider this problem next. In particular, in order to simulate scattering problems, we need an absorbing boundary condition.

2.1. Absorbing boundary condition. In this section we shall briefly develop the absorbing boundary condition of [14] since it does not appear to be well known. Suppose that all the coefficients in the Navier equation are constant and real as will usually be the case near the absorbing boundary. Let us consider a time-harmonic elastic plane wave moving in a direction $\mathbf{d}$ with $|\mathbf{d}| = 1$. The plane wave can be split into two components

$$\mathbf{u} = a_1 \mathbf{d} \exp(i\kappa_P \mathbf{x} \cdot \mathbf{d}) + a_2 \mathbf{d}^\perp \exp(i\kappa_S \mathbf{x} \cdot \mathbf{d})$$

where the wavenumbers κ_P and κ_S will be given shortly, a_1 and a_2 are constants and $\mathbf{d} \cdot \mathbf{d}^\perp = 0$. The first component denoted $\mathbf{u}_P = a_1 \mathbf{d} \exp(i\kappa_P \mathbf{x} \cdot \mathbf{d})$ is called the P-wave and we see that $\nabla \times \mathbf{u}_P = 0$ (interpreted in the scalar two dimensional sense) and that $\mathbf{u}_P$ is a solution of the Navier equation provided the wavenumber $\kappa_P = \omega / c_P$ where the wave speed for the P-wave is

$$c_P = \sqrt{\frac{\lambda + 2\mu}{\rho}}. \tag{2.7}$$

Similarly the second component of the plane wave solution, called the S-wave and given by $\mathbf{u}_S = a_2 \mathbf{d}^\perp \exp(i\kappa_S \mathbf{d} \cdot \mathbf{x})$ is a solution of the Navier equation if $\kappa_S = \omega / c_S$ and the wave speed for the S-wave is given by

$$c_S = \sqrt{\frac{\mu}{\rho}}. \tag{2.8}$$

In this case $\nabla \cdot \mathbf{u}_S = 0$.

Thus we see that the two components of the wave travel at different velocities and with different wavenumbers. An advantage of the UWVF is that these two waves can be discretized independently.

We can now develop the absorbing boundary condition. Let us first consider a simplified situation in which the domain Ω is a half space $\Omega = \{(x, y), x < 0\}$ and the boundary Γ is the line $x = 0$. A time-harmonic elastic plane wave $\mathbf{u} = (u_x, u_y)^T$, where the superscript T denotes transpose, traveling at normal incidence to the boundary Γ (i.e. with $\mathbf{d} = (1, 0)^T$) is perfectly absorbed if

$$\frac{\partial u_x}{\partial x} - i\kappa_P u_x = 0, \tag{2.9}$$

$$\frac{\partial u_y}{\partial x} - i\kappa_S u_y = 0, \tag{2.10}$$

since in this case $\mathbf{u}_P = (u_x, 0)^T$ and $\mathbf{u}_S = (0, u_y)^T$. These are the time-harmonic forms of the widely used first order absorbing boundary conditions for elastic waves, see e.g. [12] and [24].

The absorbing properties of (2.9) and (2.10) are conserved when we rewrite the boundary conditions as

$$\frac{\partial u_x}{\partial x} + \frac{c_P^2 - 2c_S^2}{c_P^2}\frac{\partial u_y}{\partial y} - i\kappa_P u_x = 0, \tag{2.11}$$

$$\frac{\partial u_y}{\partial x} + \frac{\partial u_x}{\partial y} - i\kappa_S u_y = 0. \tag{2.12}$$

These forms are particularly interesting since they allow us to relate the traction operator (2.2) and the displacement vector $\mathbf{u}$.

According to the definition of the boundary Γ the outward normal in this simplified example is $\mathbf{n} = (1, 0)^T$. It follows that the components of the traction operator $\mathbf{T}^{((1,0)^T)}(\mathbf{u}) = (T_x, T_y)^T$ are then

$$T_x = \rho c_P^2 \frac{\partial u_x}{\partial x} + \rho(c_P^2 - 2c_S^2)\frac{\partial u_y}{\partial y} \tag{2.13}$$

$$T_y = \rho c_P \left(\frac{\partial u_y}{\partial x} + \frac{\partial u_x}{\partial y} \right). \tag{2.14}$$

Combining equations (2.11)-(2.14) we formulate the absorbing boundary condition for this case as

$$\mathbf{T}^{((1,0)^T)}(\mathbf{u}) - i\sigma\mathbf{u} = 0 \tag{2.15}$$

where

$$\sigma = \begin{pmatrix} \omega\rho c_P & 0 \\ 0 & \omega\rho c_S \end{pmatrix}.$$

Correspondingly the absorbing boundary condition for a general boundary Γ with normal $\mathbf{n}$ can be derived. In that case we get

$$\mathbf{T}^{(\mathbf{n})}(\mathbf{u}) - i\sigma\mathbf{u} = 0 \tag{2.16}$$

where

$$\sigma = \omega\rho(c_P \mathbf{n} \otimes \mathbf{n} + c_S \mathbf{s} \otimes \mathbf{s}) \tag{2.17}$$

and where $\mathbf{s}$ is the tangential vector to the boundary, and $\otimes$ denotes the outer product so that $\mathbf{n} \otimes \mathbf{n} = \mathbf{n}\mathbf{n}^T$.

3. The ultra weak variational formulation of the Navier Equation. In this section we shall detail the UWVF for the elasticity problem. As in the finite element method, the UWVF starts by partitioning the domain Ω into disjoint regular finite elements K_k, $k = 1, ..., N$ of maximum radius h. We shall assume that the mesh consists of triangles, but this is not essential. Quadrilaterals can also be used, or even a mix of triangular and quadrilateral elements. The mesh must be chosen so that the coefficients λ, μ and ρ are constant on each element (of course they can be discontinuous across element boundaries). Since we let the domain Ω consist

of subdomains Ω_j (i.e. $\overline{\Omega} = \cup_{j=1}^{J} \overline{\Omega_j}$) in which material properties are constants, we require that the boundaries of the subdomains $\partial\Omega_j$ do not intersect any of the elements K_k. In other words, we require that the element edges ∂K_k coincide with the subdomain boundaries $\partial\Omega_j$.

At this stage the UWVF is just another variational formulation of the time harmonic elasticity problem and hence is not fully discrete.

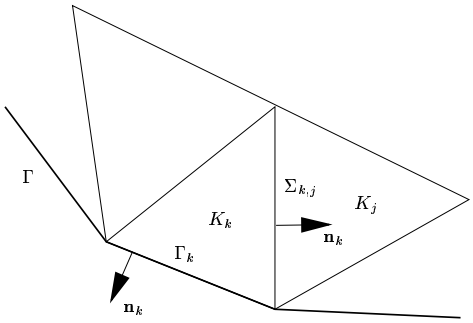

FIGURE 3.1. *A summary of the notation used to describe the UWVF mesh. The edge $\Sigma_{k,j}$ separates elements K_k and K_j with normal $\mathbf{n}_k$. Boundary edges of K_k lying on Γ (shown as a thick line) are denoted Γ_k with an outward pointing normal.*

In describing the UWVF we shall need to refer to elements and normal vectors. Let us denote by $\Gamma_k = \partial K_k \cap \Gamma$ (of course Γ_k may be empty) and by $\Sigma_{k,j} = \partial K_k \cap \partial K_j$ with normal vector pointing from K_k to K_j. Let us also denote by $\mathbf{n}_k$ the outward unit normal to element K_k. Thus the normal to $\Sigma_{k,j}$ is $\mathbf{n}_k$ and to $\Sigma_{j,k}$ is $\mathbf{n}_j = -\mathbf{n}_k$. For a graphical summary of this notation see Fig. 3.1.

Let us denote by $\mathbf{u}_k$ the restriction of $\mathbf{u}$ to K_k so that

$$\mathbf{u}_k = \mathbf{u}|_{K_k}, \tag{3.1}$$

$$\Delta^e \mathbf{u}_k + \omega^2 \rho_k \mathbf{u}_k = 0 \quad \text{in } K_k, \tag{3.2}$$

where $\rho_k = \rho|_{K_k}$ and $\lambda|_{K_k}$ and $\mu|_{K_k}$ are used in the application of Δ^e. In order to provide an appropriate boundary condition for test functions (see (3.5)), we also need to define the complex conjugate of the traction operator

$$\overline{\mathbf{T}^{(\mathbf{n})}}(\mathbf{u}) = 2\overline{\mu}\frac{\partial \mathbf{u}}{\partial n} + \overline{\lambda}\,\mathbf{n}\nabla\cdot\mathbf{u} + \overline{\mu}\,\mathbf{n}\times\nabla\times\mathbf{u} \tag{3.3}$$

where the overline indicates complex conjugation. Thus $\overline{\overline{\mathbf{T}^{(\mathbf{n})}}(\mathbf{u})} = \mathbf{T}^{(\mathbf{n})}(\overline{\mathbf{u}})$. We now prove the following "Isometry Lemma".

LEMMA 3.1. *Suppose $\mathbf{u}_k \in (H^1(K_k))^2$ is a solution of Navier's equation (3.2) on K_k such that*

$$\mathbf{T}^{(\mathbf{n}_k)}(\mathbf{u}_k) - i\sigma\mathbf{u}_k \in (L^2(\partial K_k))^2.$$

Let the test function $\mathbf{e}_k \in (H^1(K_k))^2$ satisfy

$$\Delta^e \overline{\mathbf{e}}_k + \omega^2 \rho_k \overline{\mathbf{e}}_k = 0 \quad \text{in } K_k, \tag{3.4}$$

such that

$$\overline{\mathbf{T}^{(\mathbf{n}_k)}}(\mathbf{e}_k) - i\sigma\mathbf{e}_k \in (L^2(\partial K_k))^2. \tag{3.5}$$

Then

$$\sum_k \int_{\partial K_k} \sigma^{-1}(-\mathbf{T}^{(\mathbf{n}_k)}(\mathbf{u}_k) - i\sigma\mathbf{u}_k) \cdot \overline{(-\overline{\mathbf{T}^{(\mathbf{n}_k)}}(\mathbf{e}_k) - i\sigma\mathbf{e}_k)}$$

$$= \sum_k \int_{\partial K_k} \sigma^{-1}(\mathbf{T}^{(\mathbf{n}_k)}(\mathbf{u}_k) - i\sigma\mathbf{u}_k) \cdot \overline{(\overline{\mathbf{T}^{(\mathbf{n}_k)}}(\mathbf{e}_k) - i\sigma\mathbf{e}_k)}. \tag{3.6}$$

Proof. Simply expanding the left hand side we may write

$$\begin{aligned}
&\sum_k \int_{\partial K_k} \sigma^{-1}(-\mathbf{T}^{(\mathbf{n}_k)}(\mathbf{u}_k) - i\sigma\mathbf{u}_k) \cdot \overline{(-\overline{\mathbf{T}^{(\mathbf{n}_k)}}(\mathbf{e}_k) - i\sigma\mathbf{e}_k)} \\
&= \sum_k \int_{\partial K_k} \sigma^{-1}(\mathbf{T}^{(\mathbf{n}_k)}(\mathbf{u}_k) - i\sigma\mathbf{u}_k) \cdot \overline{(\overline{\mathbf{T}^{(\mathbf{n}_k)}}(\mathbf{e}_k) - i\sigma\mathbf{e}_k)} \\
&\qquad - \sum_k 2i \int_{\partial K_k} \big(\mathbf{u}_k \cdot \overline{\overline{\mathbf{T}^{(\mathbf{n}_k)}}(\mathbf{e}_k)} - \mathbf{T}^{(\mathbf{n}_k)}(\mathbf{u}_k) \cdot \overline{\mathbf{e}}_k\big).
\end{aligned}$$

As noted above $\overline{\overline{\mathbf{T}^{(\mathbf{n}_k)}}(\mathbf{e}_k)} = \mathbf{T}^{(\mathbf{n}_k)}(\overline{\mathbf{e}}_k)$ so that using Betti's third identity [17]

$$\int_{\partial K_k} \big(\mathbf{u}_k \cdot \mathbf{T}^{(\mathbf{n}_k)}(\overline{\mathbf{e}}_k) - \mathbf{T}^{(\mathbf{n}_k)}(\mathbf{u}_k) \cdot \overline{\mathbf{e}}_k\big) = \int_{K_k} \big(\mathbf{u}_k \cdot \Delta^e \overline{\mathbf{e}}_k - \overline{\mathbf{e}}_k \cdot \Delta^e \mathbf{u}_k\big),$$

and the fact that $\mathbf{u}_k$ and $\overline{\mathbf{e}}_k$ satisfy the Navier equation we obtain

$$\begin{aligned}
\int_{\partial K_k} \big(\mathbf{u}_k \cdot \mathbf{T}^{(\mathbf{n}_k)}(\overline{\mathbf{e}}_k) - \mathbf{T}^{(\mathbf{n}_k)}(\mathbf{u}_k) \cdot \overline{\mathbf{e}}_k\big) &= \int_{K_k} \big(\mathbf{u}_k \cdot \Delta^e \overline{\mathbf{e}}_k - \overline{\mathbf{e}}_k \cdot \Delta^e \mathbf{u}_k\big) \\
&= \omega^2 \rho_k \int_{K_k} (\mathbf{u}_k \cdot \overline{\mathbf{e}}_k - \mathbf{u}_k \cdot \overline{\mathbf{e}}_k) = 0.
\end{aligned}$$

This completes the proof. ∎

By using (3.6) we can obtain the UWVF scheme. Suppose element K_j shares a boundary with element K_k. The transmission conditions (2.3) imply that

$$\mathbf{T}^{(\mathbf{n}_k)}(\mathbf{u}_k) - i\sigma\mathbf{u}_k = -\mathbf{T}^{(\mathbf{n}_j)}(\mathbf{u}_j) - i\sigma\mathbf{u}_j, \quad \text{on } \Sigma_{k,j}, \tag{3.7}$$

where we have taken into account that $\mathbf{n}_j = -\mathbf{n}_k$ on $\Sigma_{k,j}$. Using the boundary condition (2.4) on the exterior boundary Γ and substituting these into (3.6) we obtain

$$\begin{aligned}
&\sum_k \int_{\partial K_k} \sigma^{-1}\mathcal{X}_k \cdot \overline{(-\overline{\mathbf{T}^{(\mathbf{n}_k)}}(\mathbf{e}_k) - i\sigma\mathbf{e}_k)} - \sum_k \int_{\Sigma_{kj}} \sigma^{-1}\mathcal{X}_j \cdot \overline{(\overline{\mathbf{T}^{(\mathbf{n}_k)}}(\mathbf{e}_k) - i\sigma\mathbf{e}_k)} \\
&- \sum_k \int_{\Gamma_k} Q\sigma^{-1}\mathcal{X}_k \cdot \overline{(\overline{\mathbf{T}^{(\mathbf{n}_k)}}(\mathbf{e}_k) - i\sigma\mathbf{e}_k)} = \sum_k \int_{\Gamma_k} \sigma^{-1}\mathbf{g} \cdot \overline{(\overline{\mathbf{T}^{(\mathbf{n}_k)}}(\mathbf{e}_k) - i\sigma\mathbf{e}_k)}
\end{aligned} \tag{3.8}$$

where $\mathcal{X}_k = -\mathbf{T}^{(\mathbf{n}_k)}(\mathbf{u}_k) - i\sigma\mathbf{u}_k$ on ∂K_k. To clarify the variational formulation we can define the test function $\mathcal{Y}_k = -\overline{\mathbf{T}^{(\mathbf{n}_k)}}(\mathbf{e}_k) - i\sigma\mathbf{e}_k$ on ∂K_k. and define the operator $F_k : (L^2(\partial K_k))^2 \to (L^2(\partial K_k))^2$ by

$$F_k(\mathcal{Y}_k) = \overline{\mathbf{T}^{(\mathbf{n}_k)}}(\mathbf{e}_k) - i\sigma\mathbf{e}_k \tag{3.9}$$

on ∂K_k. Then the above equation gives the UWVF of finding $\mathcal{X}_k \in (L^2(\partial K_k))^2$, $k = 1, 2, ..., N$ such that

$$\sum_k \int_{\partial K_k} \sigma^{-1}\mathcal{X}_k \cdot \overline{\mathcal{Y}_k} - \sum_k \sum_j \int_{\Sigma_{k,j}} \sigma^{-1}\mathcal{X}_j \cdot \overline{F_k(\mathcal{Y}_k)}$$

$$- \sum_k \int_{\Gamma_k} Q\sigma^{-1}\mathcal{X}_k \cdot \overline{F_k(\mathcal{Y}_k)} = \sum_k \int_{\Gamma_k} \sigma^{-1}\mathbf{g} \cdot \overline{F_k(\mathcal{Y}_k)} \tag{3.10}$$

for all $\mathcal{Y}_k \in (L^2(\partial K_k))^2$, $k = 1, 2, ..., N$. This makes it clear that the unknowns in the UWVF are the traces $\mathcal{X}_k$ on ∂K_k. Of course, once these have been computed it is possible to find $\mathbf{u}$ and $\mathbf{T}^{(\mathbf{n})}(\mathbf{u})$ on ∂K_k for any k. For example, if K_k and K_j share a common boundary $\Sigma_{k,j}$ then

$$\mathbf{u}|_{\Sigma_{k,j}} = \frac{i}{2}\sigma^{-1}(\mathcal{X}_k + \mathcal{X}_j) \quad \text{and} \quad \mathbf{T}^{(\mathbf{n}_k)}(\mathbf{u}) = \frac{\mathcal{X}_j - \mathcal{X}_k}{2}. \tag{3.11}$$

A similar formula holds on the exterior boundary using the exterior boundary condition.

We have not yet given details of how to choose σ for each face. For some faces the choice of σ may be dictated by modeling considerations. For most faces it needs to be chosen as a positive definite matrix in a way that helps the conditioning of the linear system resulting from the UWVF. There are many possible choices for the coupling matrix σ. In our experience the only requirement is that entries of σ must be of the order $\omega\rho\,|c|$ where c is, for example, either c_P or c_S. Therefore on the boundary $\Sigma_{k,j}$ one could choose

$$\sigma = \omega\hat{\rho}\,\hat{c}_P\mathbf{I} \tag{3.12}$$

where $\hat{\rho}$ and $\hat{c}_P$ are mean values of ρ and $|c_P|$, respectively, across the boundary and $\mathbf{I}$ is the identity matrix. On the external boundaries $\hat{\rho}$ and $\hat{c}_P$ can be replaced with ρ and c_P, respectively.

Another possibility, more in accordance with the original philosophy of the UWVF, is to utilize the absorbing boundary condition derived in Section 2.1. Again on the internal boundaries the coupling parameter is written by means of the mean values of the moduli of the appropriate quantities if the coefficients are complex

$$\sigma = \omega\hat{\rho}(\hat{c}_P\mathbf{n} \otimes \mathbf{n} + \hat{c}_S\mathbf{s} \otimes \mathbf{s}). \tag{3.13}$$

On the exterior boundary this form reduces to (2.17) and the boundary condition reduces to the absorbing boundary condition (2.16). This is the choice we use in our codes.

4. Discretization of the UWVF. In this section we show how to discretize the UWVF developed in the previous section. Clearly we need to discretize $(L^2(\partial K_k))^2$, $1 \le k \le N$, but we need a discretization that allows us to compute the operator F_k defined in (3.9) easily. We are thus lead to use a plane wave expansion.

On each element the solution of the adjoint Navier equation (3.4) can be separated into two components using the Helmholtz decomposition

$$\mathbf{e}_k = \mathbf{e}_{k,P} + \mathbf{e}_{k,S}$$

which satisfy $\nabla \times \mathbf{e}_{k,P} = 0$ and $\nabla \cdot \mathbf{e}_{k,S} = 0$. In a homogeneous medium (i.e. on any Ω_j, $j = 1, \ldots, J$ and hence on any element K_k) the compressional (P) wave $\mathbf{e}_{k,P}$ and shear (S) wave $\mathbf{e}_{k,S}$ satisfy the Helmholtz equations

$$\Delta \overline{\mathbf{e}_{k,P}} + \kappa_P^2 \overline{\mathbf{e}_{k,P}} = 0, \tag{4.1}$$

$$\Delta \overline{\mathbf{e}_{k,S}} + \kappa_S^2 \overline{\mathbf{e}_{k,S}} = 0, \tag{4.2}$$

in K_k with the wavenumbers $\kappa_P = \omega/c_P$ and $\kappa_S = \omega/c_S$. The corresponding wave velocities c_P and c_S are functions of the Lamé constants μ, λ and the density ρ on K_k and are given, respectively, by (2.7) and (2.8). These two component waves propagate independently in the homogeneous medium in K_k but interact on the medium interfaces.

Hence, we approximate the function $\mathcal{X}_k$ using two sets of plane waves with the wave numbers κ_P and κ_S

$$\begin{aligned} \mathcal{X}_k \approx & \sum_{\ell=1}^{p_k} \left[x_{k,\ell}^P \left(-\mathbf{T}^{(\mathbf{n}_k)}(\mathbf{e}_{k,\ell}^P) - i\sigma \mathbf{e}_{k,\ell}^P \right) \right] \\ & + \sum_{\ell=1}^{s_k} \left[x_{k,\ell}^S \left(-\mathbf{T}^{(\mathbf{n}_k)}(\mathbf{e}_{k,\ell}^S) - i\sigma \mathbf{e}_{k,\ell}^S \right) \right] \end{aligned} \tag{4.3}$$

where

$$\mathbf{e}_{k,\ell}^P = \begin{cases} \mathbf{a}_{k,\ell} \exp(i\overline{\kappa}_P \mathbf{a}_{k,\ell} \cdot \mathbf{x}) & \text{in } K_k \\ 0 & \text{elsewhere} \end{cases} \tag{4.4}$$

$$\mathbf{e}_{k,\ell}^S = \begin{cases} \mathbf{a}_{k,\ell}^\perp \exp(i\overline{\kappa}_S \mathbf{a}_{k,\ell} \cdot \mathbf{x}) & \text{in } K_k \\ 0 & \text{elsewhere} \end{cases} \tag{4.5}$$

and where $\mathbf{a}_{k,\ell} = (a_{k,\ell}^1, a_{k,\ell}^2)$, $\quad |\mathbf{a}_{k,\ell}| = 1$ and $\mathbf{a}_{k,\ell}^\perp = (-a_{k,\ell}^2, a_{k,\ell}^1)$.

As advocated in earlier studies with the Helmholtz equation [5, 13], we use equispaced directions on the unit circle

$$\mathbf{a}_{k,\ell} = \left(\cos\left(2\pi \frac{\ell - 1}{q} \right), \sin\left(2\pi \frac{\ell - 1}{q} \right) \right), \quad 1 \le \ell \le q, \tag{4.6}$$

where q is the number of directions (i.e. $q = s_k$ or $q = p_k$). This is a convenient choice that guarantees convergence when the UWVF is used to approximate the Helmholtz equation. It may be that a problem specific choice of directions might furnish a more efficient basis, but this remains a topic for further research.

For $k = 1, \ldots, N$, let

$$\begin{aligned} V_{h,k} = \operatorname{span} \Big\{ & \overline{\mathbf{T}^{(\mathbf{n}_k)}}(\mathbf{e}_{k,\ell}^S) + i\sigma \mathbf{e}_{k,\ell}^S, \ 1 \le \ell \le s_k, \\ & \overline{\mathbf{T}^{(\mathbf{n}_k)}}(\mathbf{e}_{k,\ell}^P) + i\sigma \mathbf{e}_{k,\ell}^P, \ 1 \le \ell \le p_k \Big\}. \end{aligned} \tag{4.7}$$

Then the discrete UWVF problem is to compute $\mathcal{X}_{h,k} \in V_{h,k}$, $k = 1, 2, ..., N$, such that

$$\begin{aligned} & \sum_k \int_{\partial K_k} \sigma^{-1} \mathcal{X}_{h,k} \cdot \overline{\mathcal{Y}_{h,k}} - \sum_k \sum_j \int_{\Sigma_{k,j}} \sigma^{-1} \mathcal{X}_{h,j} \cdot \overline{F_k(\mathcal{Y}_{h,k})} \\ & - \sum_k \int_{\Gamma_k} Q\sigma^{-1} \mathcal{X}_{h,k} \cdot \overline{F_k(\mathcal{Y}_{h,k})} = \sum_k \int_{\Gamma_k} \sigma^{-1} \mathbf{g} \cdot \overline{F_k(\mathcal{Y}_{h,k})} \end{aligned} \tag{4.8}$$

for all $\mathcal{Y}_{h,k} \in V_{h,k}$, $k = 1, 2, ..., N$.

To obtain a discrete matrix problem corresponding to (4.8) we choose successively $\mathcal{Y}_k = \mathbf{e}^P_{k,\ell}$ and $\mathcal{Y}_k = \mathbf{e}^S_{k,\ell}$ for each k and ℓ. Substituting these into (3.8), the discrete elastic UWVF problem can be written in the matrix form

$$(I - D^{-1}C)X = D^{-1}b \tag{4.9}$$

with

$$X = (x^P_{11}, \ldots, x^P_{1p_1}, x^S_{11} \ldots, x^S_{1s_1}, \ldots)^T.$$

The matrix D is a block-diagonal matrix in which each block D^k consists of four sub-blocks

$$D = \begin{pmatrix} D^1 & 0 & \ldots & \ldots & 0 \\ 0 & \ddots & 0 & \ldots & 0 \\ \vdots & 0 & D^k & 0 & 0 \\ \vdots & \vdots & 0 & \ddots & 0 \\ 0 & 0 & 0 & 0 & D^N \end{pmatrix}$$

where

$$D^k = \begin{pmatrix} D^k_1 & D^k_2 \\ D^k_3 & D^k_4 \end{pmatrix}$$

with the elements

$$D^k_{1,\ell,m} = \int_{\partial K_k} \sigma^{-1}\big(-\mathbf{T}^{(\mathbf{n}_k)}(\mathbf{e}^P_{k,m}) - i\sigma\mathbf{e}^P_{k,m}\big) \cdot \overline{\big(-\overline{\mathbf{T}^{(\mathbf{n}_k)}}(\mathbf{e}^P_{k,\ell}) - i\sigma\mathbf{e}^P_{k,\ell}\big)},$$

$$D^k_{2,\ell,m} = \int_{\partial K_k} \sigma^{-1}\big(-\overline{\mathbf{T}^{(\mathbf{n}_k)}}(\mathbf{e}^S_{k,m}) - i\sigma\mathbf{e}^S_{k,m}\big) \cdot \overline{\big(-\overline{\mathbf{T}^{(\mathbf{n}_k)}}(\mathbf{e}^P_{k,\ell}) - i\sigma\mathbf{e}^P_{k,\ell}\big)},$$

$$D^k_{3,\ell,m} = \int_{\partial K_k} \sigma^{-1}\big(-\overline{\mathbf{T}^{(\mathbf{n}_k)}}(\mathbf{e}^P_{k,m}) - i\sigma\mathbf{e}^P_{k,m}\big) \cdot \overline{\big(-\overline{\mathbf{T}^{(\mathbf{n}_k)}}(\mathbf{e}^S_{k,\ell}) - i\sigma\mathbf{e}^S_{k,\ell}\big)},$$

$$D^k_{4,\ell,m} = \int_{\partial K_k} \sigma^{-1}\big(-\mathbf{T}^{(\mathbf{n}_k)}(\mathbf{e}^S_{k,m}) - i\sigma\mathbf{e}^S_{k,m}\big) \cdot \overline{\big(-\overline{\mathbf{T}^{(\mathbf{n}_k)}}(\mathbf{e}^S_{k,\ell}) - i\sigma\mathbf{e}^S_{k,\ell}\big)}.$$

The matrix C is also a block matrix with the blocks C^k on the diagonal and $C^{k,j}$ off the diagonal where

$$C^k = \begin{pmatrix} C^k_1 & C^k_2 \\ C^k_3 & C^k_4 \end{pmatrix}, \quad \text{and} \quad C^{k,j} = \begin{pmatrix} C^{k,j}_1 & C^{k,j}_2 \\ C^{k,j}_3 & C^{k,j}_4 \end{pmatrix}.$$

The elements of the blocks are

$$C^k_{1,\ell,m} = \int_{\Gamma_k} Q\sigma^{-1}\big(-\mathbf{T}^{(\mathbf{n}_k)}(\mathbf{e}^P_{k,m}) - i\sigma\mathbf{e}^P_{k,m}\big) \cdot \overline{\big(\overline{\mathbf{T}^{(\mathbf{n}_k)}}(\mathbf{e}^P_{k,\ell}) - i\sigma\mathbf{e}^P_{k,\ell}\big)},$$

$$C^k_{2,\ell,m} = \int_{\Gamma_k} Q\sigma^{-1}\big(-\mathbf{T}^{(\mathbf{n}_k)}(\mathbf{e}^S_{k,m}) - i\sigma\mathbf{e}^S_{k,m}\big) \cdot \overline{\big(\overline{\mathbf{T}^{(\mathbf{n}_k)}}(\mathbf{e}^P_{k,\ell}) - i\sigma\mathbf{e}^P_{k,\ell}\big)},$$

$$C^k_{3,\ell,m} = \int_{\Gamma_k} Q\sigma^{-1}\big(-\mathbf{T}^{(\mathbf{n}_k)}(\mathbf{e}^P_{k,m}) - i\sigma\mathbf{e}^P_{k,m}\big) \cdot \overline{\big(\overline{\mathbf{T}^{(\mathbf{n}_k)}}(\mathbf{e}^S_{k,\ell}) - i\sigma\mathbf{e}^S_{k,\ell}\big)},$$

$$C^k_{4,\ell,m} = \int_{\Gamma_k} Q\sigma^{-1}\big(-\mathbf{T}^{(\mathbf{n}_k)}(\mathbf{e}^S_{k,m}) - i\sigma\mathbf{e}^S_{k,m}\big) \cdot \overline{\big(\overline{\mathbf{T}^{(\mathbf{n}_k)}}(\mathbf{e}^S_{k,\ell}) - i\sigma\mathbf{e}^S_{k,\ell}\big)},$$

and

$$C^{k,j}_{1,\ell,m} = \int_{\Sigma_{kj}} \sigma^{-1}\big(\mathbf{T}^{(\mathbf{n}_k)}(\mathbf{e}^P_{j,m}) - i\sigma\mathbf{e}^P_{j,m}\big)\cdot\overline{\big(\overline{\mathbf{T}^{(\mathbf{n}_k)}}(\mathbf{e}^P_{k,\ell}) - i\sigma\mathbf{e}^P_{k,\ell}\big)},$$

$$C^{k,j}_{2,\ell,m} = \int_{\Sigma_{kj}} \sigma^{-1}\big(\mathbf{T}^{(\mathbf{n}_k)}(\mathbf{e}^S_{j,m}) - i\sigma\mathbf{e}^S_{j,m}\big)\cdot\overline{\big(\overline{\mathbf{T}^{(\mathbf{n}_k)}}(\mathbf{e}^P_{k,\ell}) - i\sigma\mathbf{e}^P_{k,\ell}\big)},$$

$$C^{k,j}_{3,\ell,m} = \int_{\Sigma_{kj}} \sigma^{-1}\big(\mathbf{T}^{(\mathbf{n}_k)}(\mathbf{e}^P_{j,m}) - i\sigma\mathbf{e}^P_{j,m}\big)\cdot\overline{\big(\overline{\mathbf{T}^{(\mathbf{n}_k)}}(\mathbf{e}^S_{k,\ell}) - i\sigma\mathbf{e}^S_{k,\ell}\big)},$$

$$C^{k,j}_{4,\ell,m} = \int_{\Sigma_{kj}} \sigma^{-1}\big(\mathbf{T}^{(\mathbf{n}_k)}(\mathbf{e}^S_{j,m}) - i\sigma\mathbf{e}^S_{j,m}\big)\cdot\overline{\big(\overline{\mathbf{T}^{(\mathbf{n}_k)}}(\mathbf{e}^S_{k,\ell}) - i\sigma\mathbf{e}^S_{k,\ell}\big)}.$$

The entries of the matrices C and D can be computed exactly since they only involve integrals of complex exponentials along lines. The linear system (4.9) is then solved by applying the bi-conjugate gradient scheme.

After the vector X is computed, the solution $\mathcal{X}_k$ on ∂K_k can be approximated using (4.3) and the traction and displacement approximated by using (3.11).

5. Analysis of the elastic UWVF method. The method of analysis for the acoustic UWVF presented in [5] applies to the elastic UWVF with very minor changes. We now present an application of this theory to the elastic UWVF with sufficient details to make this claim obvious. Unfortunately the final error estimate is not currently available due to the need to analyze the approximation properties of the elastic plane wave basis functions.

As in [5] we consider the simple case where all the coefficients in the problem are real and constant. Thus we assume λ, μ, ρ and ω are real and constant, and we choose $\sigma = 1$. The theory can be extended to more general piecewise constant coefficients. The domain Ω is assumed to be a Lipschitz (and in practice a Lipschitz polygon).

First we need a global solution space. Thus we define $V = \Pi_{k=1}^N (L^2(\partial K_k))^2$ with the inner product

$$(\mathbf{u},\mathbf{v})_V = \sum_{k=1}^N \int_{\partial K_k} \mathbf{u}\cdot\overline{\mathbf{v}}\, ds$$

and the norm $\|\mathbf{u}\|_V^2 = \sqrt{(\mathbf{u},\mathbf{u})_V}$. Even though this space depends on the mesh, we do not indicate this explicitly since this is the space for the continuous solution of (3.10). However the fact that V depends on the mesh complicates the analysis. Now we need a global operator $F : V \to V$ defined such that if $\mathcal{Y} = (\mathcal{Y}_1,\ldots,\mathcal{Y}_N)^T \in V$ then

$$F(\mathcal{Y})|_{\partial K_k} = F_k(\mathcal{Y}_k), \quad 1 \le k \le N,$$

where F_k is defined in (3.9). Let $\|F\|_{V\to V}$ denote the operator norm of F. The main result underlying the analysis is the following, which also explains why Lemma 3.1 is called the "Isometry Lemma".

LEMMA 5.1. *Assuming that the coefficients in the elastic UWVF are real and constant and that $\sigma = 1$, the operator F is an isometry so that $\|F\|_{V\to V} = 1$, and $F^*F = I$ where F^* is the adjoint of F in the V-inner product.*

Proof. Let us define $\mathbf{e}_k \in (H^1(K_k))^2$ to be the weak solution of

$$\begin{aligned} &\Delta^e\mathbf{e}_k + \omega^2\rho\mathbf{e}_k = 0 \quad \text{in } K_k,\\ &\mathbf{T}^{\mathbf{n}_k}(\mathbf{e}_k) + i\mathbf{e}_k = -\mathcal{Y}_k \quad \text{on } \partial K_k. \end{aligned}$$

Then using the Isometry Lemma, and noting that since all coefficients are real we can remove the complex conjugation in (3.4) we obtain

$$\begin{aligned}\|F(\mathcal{Y})\|_V^2 &= \sum_{k=1}^{N} \|\mathbf{T}^{\mathbf{n}_k}(\mathbf{e}_k) - i\mathbf{e}_k\|^2_{(L^2(\partial K_k))^2} \\ &= \sum_{k=1}^{N} \| - \mathbf{T}^{\mathbf{n}_k}(\mathbf{e}_k) - i\mathbf{e}_k\|^2_{(L^2(\partial K_k))^2} \\ &= \sum_{k=1}^{N} \|\mathcal{Y}_k\|^2_{(L^2(\partial K_k))^2} = \|\mathcal{Y}\|_V^2.\end{aligned}$$

This proves the isometry and since this holds for all $\mathcal{Y} \in V$ we obtain the property that $F^*F = I$. ∎

The final component of the analysis is an operator that corresponds to (3.7). Thus we define $\pi : V \to V$ such that if $\mathcal{Y} \in V$ then

$$\pi\mathcal{Y}|_{\Sigma_{k,j}} = \mathcal{Y}|_{\Sigma_{j,k}} \quad \text{for } 1 \le k, j \le N, \text{ on interior edges,} \tag{5.1}$$

$$\pi\mathcal{Y}|_{\Gamma_k} = Q\mathcal{Y}|_{\Gamma_k} \quad \text{for } 1 \le k \le N, \text{ on the boundary } \Gamma. \tag{5.2}$$

Thus, for an interior edge, π just swaps the boundary data across an edge, while on the boundary Γ the boundary data is used. With this definition we see that if $\mathcal{G} \in V$ is defined by

$$\mathcal{G} = \begin{cases} \mathbf{g} & \text{on } \Gamma_k \\ 0 & \text{on } \Sigma_{k,j} \end{cases} \qquad 1 \le k, j \le N.$$

then we may rewrite (3.10) as the problem of finding $\mathcal{X} = (\mathcal{X}_1, \ldots, \mathcal{X}_N)^T \in V$ such that

$$(\mathcal{X}, \mathcal{Y})_V - (\pi\mathcal{X}, F(\mathcal{Y}))_V = (\mathcal{G}, F(\mathcal{Y}))_V \quad \text{for all } \mathcal{Y} \in V.$$

Using the adjoint operator F^* this can be written as the problem of finding $\mathcal{X} \in V$ such that

$$(I - F^*\pi)\mathcal{X} = F^*\mathcal{G}$$

and we can now see that, written as an operator equation, the elastic UWVF has the same form as the acoustic UWVF in [5].

We next examine the properties of π defined in (5.1)-(5.2).

LEMMA 5.2. *Provided $|Q| \le 1$, the operator π satisfies the following estimate*

$$\|\pi\mathcal{Y}\|_V^2 = \int_\Gamma (|Q|^2 - 1)|\mathcal{Y}|^2 \, ds + \|\mathcal{Y}\|_V^2.$$

The proof of this result follows exactly the corresponding result in [5]. The slightly contractive property of π when $|Q| < 1$ allows us to prove error estimates on Γ. Now that we have verified all the properties of π and F necessary for the UWVF theory from [5] we may summarize a basic existence result for the continuous elastic UWVF as follows.

THEOREM 5.3. *The continuous problem (3.10) has a unique solution provided* $|Q| < 1$. *If* $|Q| = 1$ *the problem has a solution provided* ω *is not an eigenfrequency of* Ω *for the resonance problem associated with (2.1), (2.3) and (2.4).*

We now consider the discrete solution of the UWVF problem. Let $V_h = \Pi_{k=1}^N V_{h,k}$ where $V_{h,k}$ is given by (4.7) and we assume that the directions of the plane waves on each element are uniformly distributed as in (4.6). Let $P_h : V \to V_h$ denote the V projection onto V_h so that for any $\mathcal{Z} \in V$, we define $P_h\mathcal{Z} \in V_h$ by

$$(P_h\mathcal{Z} - \mathcal{Z}, \mathcal{Y}_h)_V = 0 \quad \text{for all } \mathcal{Y}_h \in V_h.$$

The discrete elastic UWVF (4.8) may now be written as the problem of finding $\mathcal{X}_h \in V_h$ such that

$$(\mathcal{X}_h, \mathcal{Y}_h)_V - (\pi\mathcal{X}_h, F(\mathcal{Y}_h))_V = (\mathcal{G}, F(\mathcal{Y}_h))_V \quad \text{for all } \mathcal{Y}_h \in V_h,$$

and in terms of operators can be written as

$$(I - P_h F^* \pi)\mathcal{X}_h = P_h F^*(\mathcal{G}).$$

Using the forgoing properties of F and π, the results of [5] show that if Q is chosen so that there is a constant δ such that $|Q| \leq \delta < 1$ then

$$\|\mathcal{X} - \mathcal{X}_h\|_{(L^2(\Gamma))^2} \leq \frac{2}{\sqrt{1-\delta^2}} \|\mathcal{X} - P_h\mathcal{X}\|_V.$$

On the one hand this estimate is lacking in that it does not allow us to estimate the error of the discrete UWVF away from Γ and it does not allow the important case $|Q| = 1$. On the other hand the constant in the estimate is quite specific. Unfortunately the approximation properties of $P_h\mathcal{X}$ are not available yet. We expect that an estimate similar to that proved in [5] can be proved in this case by an extension of the method there. However, in this paper we focus on the development of the algorithm and numerical tests. In particular the numerical tests shown in the next section suggest that $\|\mathcal{X} - \mathcal{X}_h\|_{(L^2(\Gamma))^2} = O(h^\alpha)$ for some constant α that increases as the minimum number of directions per element increases. We hope to prove this in future.

6. Numerical results.

6.1. Wave propagation. For first example we study elastic wave propagation through a rectangular domain $\Omega = [0,1] \times [0,1]$. The exact solution is a plane wave consisting both P- and S-waves

$$\mathbf{u}^{\text{inc}} = \alpha\mathbf{a}\exp(i\kappa_P\mathbf{a}\cdot\mathbf{x}) + \beta\mathbf{b}\exp(i\kappa_S\mathbf{a}\cdot\mathbf{x}). \tag{6.1}$$

The directions $\mathbf{a}$ and $\mathbf{b}$ are chosen so that $\alpha, \beta \in \mathbb{R}$ and $\mathbf{a}\cdot\mathbf{b} = 0$. This example is chosen because it provides a very simple problem to test the accuracy of the elastic UWVF for wave propagation.

Elastic properties of the medium occupying the domain Ω are taken to be those of steel ($E = 200\cdot 10^9$, $\nu = 0.3$ and $\rho = 7800$). Hence, S- and P-wave speeds are $c_P = 5875$ and $c_S = 3140$, respectively. This gives a ratio $c_P/c_S = \kappa_S/\kappa_P = 1.87$. Single frequency examples for this first model problem are computed with $f = 2.0\cdot 10^4$ which corresponds to $\kappa_P = 21.4$. These parameters are not motivated by any particular application but the ratio c_P/c_S is typical for a wide range of solid materials.

The direction of the wave in all cases is $\mathbf{a} = (\cos(\pi/\tilde{q}), \sin(\pi/\tilde{q}))^T$ where $\tilde{q} = \max(p_k, s_k)$. This choice does not coincide with any of the directions of the plane wave basis functions $\mathbf{a}_{k,\ell}$. Furthermore, we choose the amplitudes of the incident waves in all examples to be $\alpha = 1$ and $\beta = 1$. The source term can be given now in the form

$$\mathbf{g} = (1+Q)\mathbf{T}^{(\mathbf{n})}(\mathbf{u}^{\text{inc}}) - i\sigma(1-Q)\mathbf{u}^{\text{inc}} \quad \text{on } \Gamma, \tag{6.2}$$

and we choose $Q = 0.1$. The coupling parameter σ is given by (2.17).

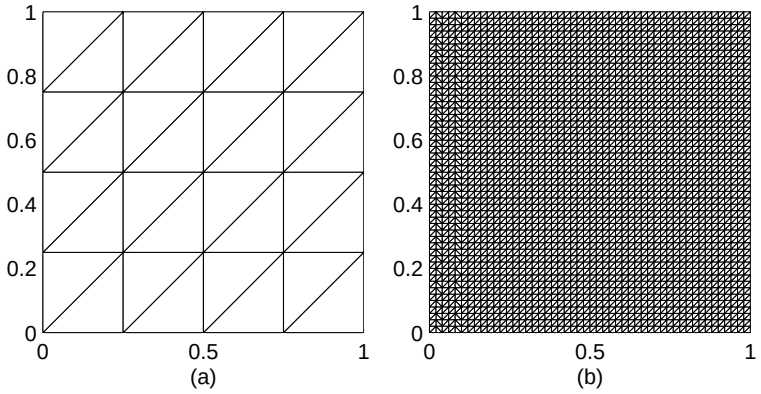

FIGURE 6.1. *Left: A typical uniform mesh used in UWVF simulations. Right: A mesh for the FEM simulations. For the material properties and frequency used in the wave propagation study, the ratio of P-wavelength and mesh parameter λ_P/h is 0.83 for the mesh (a) and 10.38 for the mesh (b).*

Typical meshes used in simulations are shown in Fig. 6.1. Obviously, in this example, we use uniform meshes so the number of P- and S-wave basis functions per element (p_k and s_k) can be chosen independent of k. However, due to the difference in the P- and S-wavenumbers, there may be an advantage to choosing different values for p_k and s_k. Thus we begin by studying how the choice of basis affects the accuracy and the stability of the elastic UWVF approximation. In this and later studies we compute the error in a discrete relative least squares norm as follows. First we average the UWVF results at the nodes to obtain nodal values of the displacement (this is motivated by our desire to compare to the FEM later). The discrete least squares norm error is simply the unweighted sum of the squares of the nodal error.

In the top panel of Fig. 6.2 we show the error in the computed solution using the analytical solution $\mathbf{u} = \mathbf{u}^{\text{inc}}$ (see (6.1)) with various ratios s_k/p_k and increasing the number of directions per element to give more degrees of freedom. The results suggest that the ratio of the number of S- and P-wave basis functions (s_k/p_k) should be approximately κ_S/κ_P in order to obtain the best accuracy. In addition the bottom panel of Fig. 6.2 shows the conditioning of the $I - D^{-1}C$ corresponding to the computations shown in the top panel. The choice that s_k/p_k should be of the order of κ_S/κ_P also improves the conditioning of the linear system in most cases (except for very large numbers of degrees of freedom). Thus, both from the point of view of accuracy and from the point of view of the stability of the method, we should choose the ratio s_k/p_k in the manner just described.

The behavior of the error and conditioning as a function of $1/h$ for a fixed number of basis functions per element (i.e. fixed p_k and s_k) and variable mesh size is presented

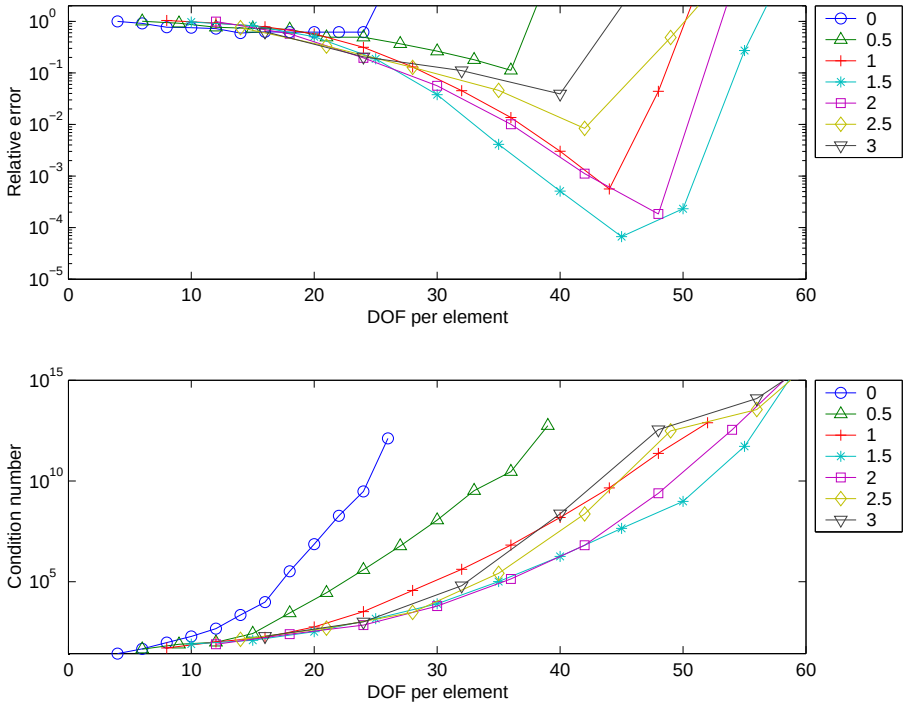

FIGURE 6.2. *Relative error and condition number of* $I - D^{-1}C$ *as a function of the number of degrees of freedom (DOF) per element for different ratios* s_k/p_k. *Results are computed in the mesh of Fig. 6.1 (a). The frequency is* $f = 2.0 \cdot 10^4$ *and* $\kappa_S/\kappa_P = 1.87$. *The eventual blowup of relative error in the top figure is due to the increase in condition number with the number of degrees of freedom.*

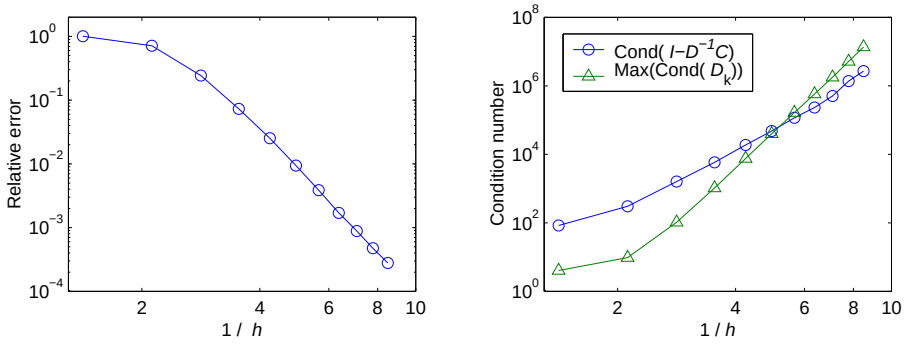

FIGURE 6.3. *Relative error (left) and condition number (right) as a function of the mesh parameter* $1/h$. *Results are computed with* $\kappa_P = 21.4$, $p_k = 10$ *and* $s_k/p_k = 1.5$.

in Fig. 6.3. From the left panel we can see that the error decreases $O(h^\alpha)$ for $\alpha \approx 6.4$ provided h is small enough. From the right hand panel of Fig. 6.3 we can see that the maximum condition number of the matrix blocks D_k gives a good indication of the condition number of the system matrix $I - D^{-1}C$ and hence, can be used as a predictor of the conditioning of the system matrix. Obviously it is much easier to compute the condition number of the diagonal blocks of D than of the entire matrix

$I - D^{-1}C$. Previously, this property has been utilized for choosing a stable set of basis functions for the Helmholtz problem [13]. In practice we use a similar approach for the elastic UWVF.

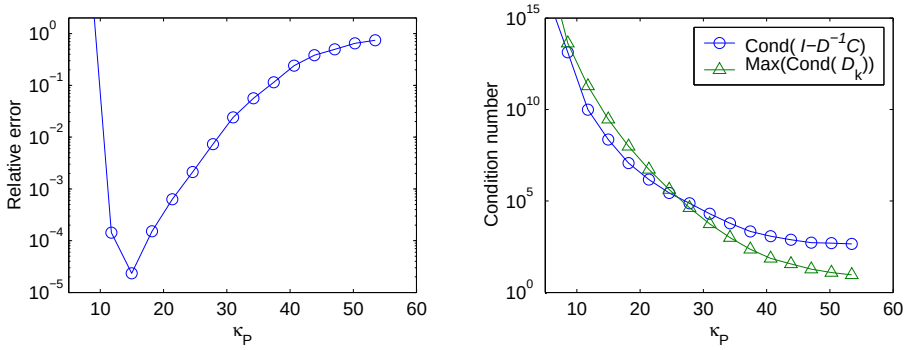

FIGURE 6.4. *Relative error and condition number as a function of the wavenumber κ_P when $p_k = 16$ and $s_k/p_k = 1.5$. Results are computed in the mesh of Fig. 6.1 (a)*

Next, in Fig. 6.4, we examine the behavior of the elastic UWVF on a fixed mesh with a fixed basis, but varying ω so that κ_P and κ_S both vary while keeping κ_S/κ_P fixed. In particular we plot relative error and condition number as a function of κ. Note that in [19] a non-dimensional incremental wave number that includes both the mesh size h and number of directions of the plane waves is proposed. For the Helmholtz equation this incremental wave number is then related to the condition number. We have elected to use the ordinary wave number κ to present our results since h, and the number of wave directions are fixed. In addition it is necessary to study the relationship of the condition number and the incremental wave number anew for elasticity which involves two wave-speeds.

For low κ_P the conditioning of the UWVF matrix $I - D^{-1}C$ is very poor since all plane waves are almost constant on each element. As κ_P increases, the conditioning improves and an accurate solution is obtained. As κ_P increases further, the error then increases as can be expected from analyzing how a plane wave is approximated by a sum of other plane waves not traveling in the same direction. It is again useful to note (from the right hand panel of this figure) that the maximum condition number of the blocks of D is a good estimate of the condition number of the overall system matrix.

Finally, we compare the piecewise linear finite element method (FEM) with the UWVF for the same wave propagation problem. In particular the FEM used here is a displacement formulation using natural boundary conditions equivalent to (2.4). The discrete relative least squares error in the FEM solution against the reciprocal of the element size $1/h$, for a fixed frequency and wavenumber, are shown in the left hand panel of Fig. 6.5. The solution converges with an error that is $O(h^2)$ as is to be expected for the piecewise linear FEM. Comparing the left panel of this figure with the left hand panel of Fig. 6.3, it is obvious that much finer meshes are needed in the finite element scheme than in the UWVF to obtain equal accuracy. In the right hand panel we examine the dependence of the error of the FEM solution on the wavenumber κ_P (keeping the ratio κ_S/κ_P fixed). As is to be expected, the error increases with κ_P (due to accumulating phase error). Compared to the right hand panel of Fig. 6.4 we see that the finite element method is free from the low frequency

conditioning problem that afflicts the UWVF.

Even though the FEM requires a much finer grid than the UWVF to obtain similar accuracy, we need to be careful in comparing the efficiency of the two schemes because the UWVF has multiple degrees of freedom per element. To try to compare the methods more directly, we show in Fig. 6.6 a plot of the error in the FEM and UWVF schemes as a function of the number of non-zero entries in the resulting matrices. We consider both the h-UWVF where we fix the basis on each element and decrease the mesh size h to obtain an accurate solution, and the p-UWVF where we increase the number of directions per element on a fixed mesh. Using either strategy the resulting matrix system is more dense in the UWVF than in the FEM. However, the overall storage needed to reach a desired accuracy is lower for the UWVF than for the FEM (see Fig. 6.6). Perhaps this not surprising since the solution is smooth and hence a higher order method (like UWVF) should be more efficient than a low order method like FEM.

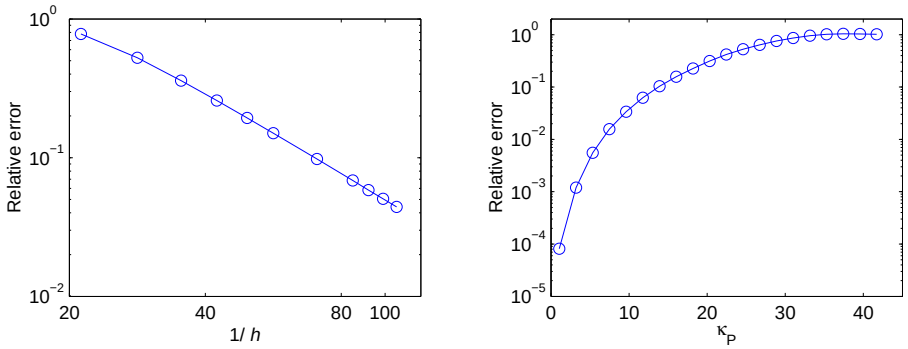

FIGURE 6.5. *Left: A log-log plot of the relative error as a function of the mesh parameter* $1/h$ *in the finite element scheme. Results are shown for* $f = 2.0 \cdot 10^4$*, i.e.* $\kappa_P = 21.4$*. Right: Relative error against the wavenumber* κ_P *in the mesh of Fig. 6.1 (b).*

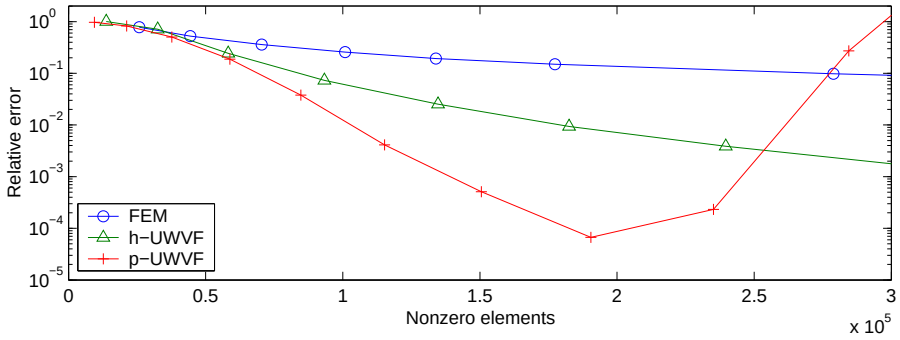

FIGURE 6.6. *Relative error as a function of storage, i.e. the number of nonzero elements in resulting matrix system. The abbreviation FEM refers to the piecewise linear finite element method; h-UWVF to the elastic UWVF with constant number of basis functions* ($p_k = 10$ *and* $s_k/p_k = 1.5$) *and varying element size h; and p-UWVF to the elastic UWVF with fixed mesh (the mesh of Fig. 6.1 (a) and* $s_k/p_k = 1.5$*) and varying number of basis functions* p_k*. Results are for* $f = 2 \cdot 10^4$*.*

The results from this example suggest a number of conclusions which we offer under the caveat that they are not proven and are based on a small set of elasticity

examples. However they are supported by our experience with the UWVF and FEM for other problems:

- The UWVF compares well to the piecewise linear FEM.
- It is desirable to choose the number of S- and P-wave directions depending on the ratio κ_P/κ_S to improve both the accuracy and conditioning of the elastic UWVF.
- The conditioning of the linear system resulting from the UWVF can be estimated from the conditioning of the diagonal blocks of D. Hence the basis on each element may be chosen locally and still provide control over the overall condition number.
- The accuracy of the UWVF, for a fixed mesh and element-wise basis, deteriorates as the frequency ω increases, thus we see that the UWVF does not escape from buildup of phase error that afflicts the FEM.

6.2. Rayleigh waves. Near material boundaries, edge or surface waves can be generated. These waves travel along the boundary but decay rapidly into the bulk. Perhaps the simplest example of surface waves are Rayleigh waves that can be generated at a free surface (i.e. where $\mathbf{T}^{(\mathbf{n})}(\mathbf{u}) = 0$).

Since discretization of the UWVF method in this study uses P- and S-plane waves only, it is vital to investigate whether the method can resolve surface waves that are not explicitly contained in the basis for the UWVF. To do this we study Rayleigh waves on the surface of a semi-infinite elastic half-space. This is done by considering a portion of the half-space and using appropriate boundary data. More precisely, the computational domain is the square $\Omega = [0,1] \times [0,1]$ having Rayleigh waves propagating along the $y = 0$ surface in the direction of the positive x-axis. The material properties of the medium and the frequency of the wave field $f = 2 \cdot 10^4$ are the same as in the first test problem in Section 6.1.

The exact expression for the Rayleigh wave speed c_R is somewhat complicated, therefore we use the approximate value from [2] given by

$$c_R = \frac{0.87 + 1.12\nu}{1 + \nu} c_S$$

where ν is the Poisson ratio. For our examples $\nu = 0.3$, and the accuracy of this approximation is better than 0.5 %. In addition, we denote the Rayleigh wave number by $\kappa_R = \omega/c_R$. In this example, the wave speed c_R and wave number κ_R are 2913 and 43.1, respectively.

The x and y components of the displacement field $\mathbf{u} = (u_x, u_y)^T$ can be written as follows (see e.g. [2] for details)

$$u_x = \alpha_S \left\{ e^{-\alpha_S y} - \frac{2\kappa_R^2}{\kappa_R^2 + \alpha_S^2} e^{-\alpha_P y} \right\} e^{i\kappa_R x}, \tag{6.3}$$

$$u_y = i\kappa_R \left\{ e^{-\alpha_S y} - \frac{2\alpha_P \alpha_S}{\kappa_R^2 + \alpha_S^2} e^{-\alpha_P y} \right\} e^{i\kappa_R x}, \tag{6.4}$$

where

$$\alpha_P = \sqrt{\kappa_R^2 - \left(\frac{\omega}{c_P}\right)^2} \quad \text{and} \quad \alpha_S = \sqrt{\kappa_R^2 - \left(\frac{\omega}{c_S}\right)^2}.$$

This solution of the Rayleigh wave problem is shown in Fig. 6.7. The trajectories of the particle motion in the field are ellipses whose major axes are normal to the surface.

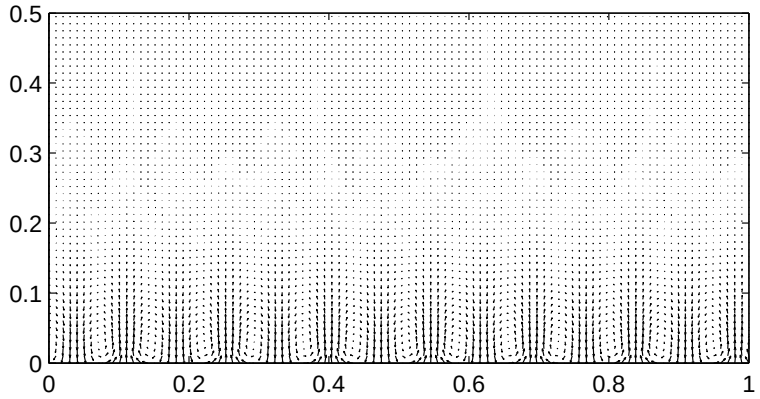

FIGURE 6.7. *The exact solution of the Rayleigh wave problem in the neighborhood of the free surface.*

The UWVF approximation of the Rayleigh wave solution (6.3) and (6.4) is obtained by using the Rayleigh wave field as the incident field $\mathbf{u}^{\text{inc}}$ in equation (6.2) taking $Q = 0.1$, except on the edge $y = 0$ where $Q = 1$ in order to obtain a traction free boundary condition there. This provides a boundary condition on the boundary of the computational domain Ω. In Fig. 6.8 we show the relative error of the UWVF approximation of the Rayleigh wave as a function of the mesh size parameter $1/h$. To enable comparison with the previous computations, we also plot the error for approximating the combined S- and P-wave solution from Section 6.1. The result clearly shows that the S- and P-wave basis used in the UWVF can approximate Rayleigh waves, even though Rayleigh waves are not contained in the basis. However, for a given mesh, the accuracy is degraded compared to approximating a pure combination of S- and P- waves (note that for this example the wavelength of the P-wave is roughly twice that of the Rayleigh wave). The same reduced accuracy can be observed in the plot of the error as a function of wave number κ_P (Fig. 6.9). These results suggest that it may be useful to refine the grid or increase the number of plane waves in the basis close to free boundaries, but this suggestion needs to be investigated further.

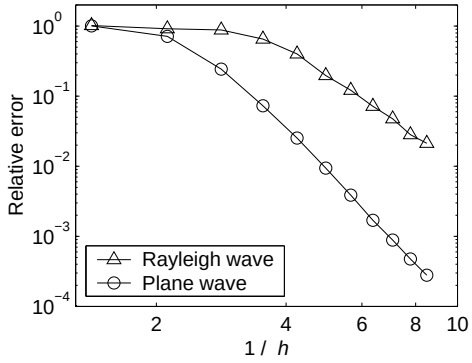

FIGURE 6.8. *The accuracy of the UWVF approximation for the Rayleigh and plane wave solutions as a function of mesh size parameter* $1/h$. *In both cases are computed with* $f = 2 \cdot 10^4$, $p_k = 10$ *and* $s_k/p_k = 1.5$.

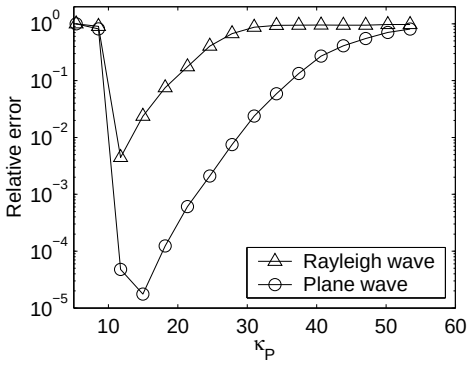

FIGURE 6.9. *The accuracy of the UWVF approximation for the Rayleigh and plane wave solutions as a function of the wave number κ_P. The computations are done in the mesh of Fig. 6.1 (a) with $p_k = 16$ and $s_k/p_k = 1.5$.*

TABLE 6.1
Material properties

Ex.	Figs.	Domain	E	ν	ρ	c_P	c_S	c_P/c_S
1	6.10-6.11	$r < 0.5$	$200 \cdot 10^9$	0.30	7800	5875	3140	1.87
		$0.5 \leq r \leq 1.0$	$200 \cdot 10^9$	0.47	7800	12413	2953	4.20
2	6.12-6.13	$r < 0.5$	$200 \cdot 10^9$	0.30	7800	5875	3140	1.87
		$0.5 \leq r \leq 1.0$	$14 \cdot 10^9$	0.25	1800	3055	1763	1.73

6.3. Transmission. As a third model problem we analyze the transmission of elastic plane waves through a circular inhomogeneity with radius $r = 0.5$ embedded in an infinite homogeneous background material. A similar problem has been studied, for example, in [20]. Since the problem is physically unbounded, we truncate the computational domain by another circle with radius $r = 1$ where we use the absorbing boundary condition developed in Section 2.1. We analyze transmission in two examples for which the material properties of the inhomogeneities and backgrounds are shown in Table 6.3. In all simulations the frequency is $f = 1.0 \cdot 10^4$.

The incoming wave is of the form (6.1). In some examples, however, we study separately cases with incident P- and S-waves. The direction of propagation of the incident wave in both cases is $\mathbf{a} = (1, 0)$.

We approximate the problem in the ultra weak scheme by using (2.17) as the coupling parameter, setting $Q = 0$ and

$$\mathbf{g} = \mathbf{T}^{(\mathbf{n})}(\mathbf{u}^{\text{inc}}) - i\sigma\mathbf{u}^{\text{inc}} \quad \text{on } \Gamma.$$

If we assume that the solution of the problem now consists of the incoming and scattered fields $\mathbf{u} = \mathbf{u}^{\text{inc}} + \mathbf{u}^{\text{sc}}$, these particular choices correspond to the first order absorbing boundary condition (2.16) for the scattered part $\mathbf{u}^{\text{sc}}$.

For comparison, an accurate approximation to the physical transmission problem is computed using a truncated Fourier-Bessel series. This method is described in full detail in [20]. We truncate the infinite Fourier series when the relative change of solution due to an additional Fourier mode is less than 10^{-5}.

There are three sources of error in the UWVF calculation. First, we are computing on a bounded domain with an absorbing boundary condition. This is probably the

main source of error. Second, the interior circle is approximated using a polyhedral approximation. In our work on the Helmholtz equation we have implemented the UWVF with curved boundaries and that work needs to be extended to the elastic UWVF. There is no fundamental difficulty with doing this except that during matrix assembly integrals on curved sections need to be approximated by quadrature, so slowing the assembly procedure. Finally, of course, there is the approximation error due to discretizing the problem on the bounded domain by the UWVF. Due to the first two approximations a discrepancy of the order $5-15\%$ can be expected between the UWVF and Fourier series approximations even for very fine grids or large numbers of directions per element. In fact, we see that the asymptotic error of the method is around 10%.

Because the mesh, shown in Fig 6.10, is unstructured and the elastic properties depend on position it is helpful to vary the total number of basis functions, and the ratio of S- and P-wave basis functions element by element. Since the accuracy of the UWVF approximation depends on both of these factors, we analyze them separately. In the first part of the study, we fix the ratio of the S- and P-wave basis functions, and seek a feasible method to choose the total number of basis functions in each element. In the second part of the study, we show the effect of the S- and P-wave composition of the basis functions on the UWVF approximation.

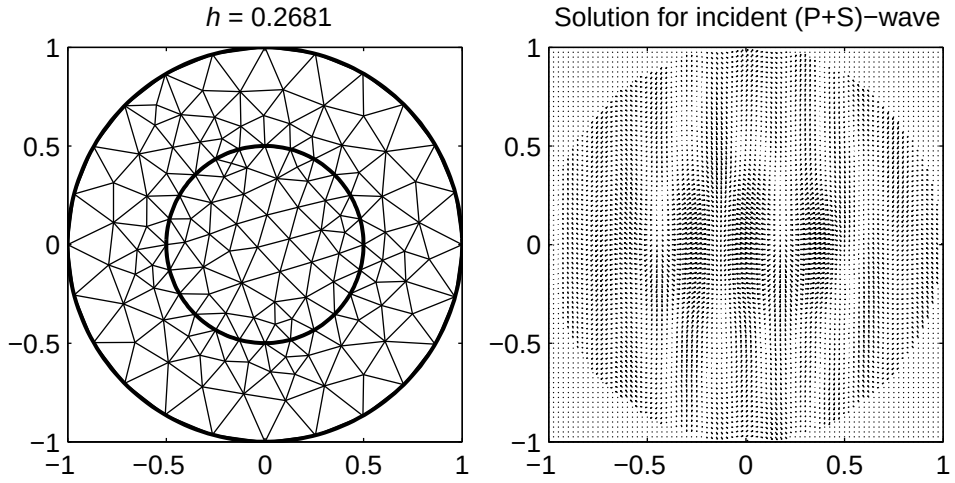

FIGURE 6.10. Left: *The mesh used for the transmission problem.* Bottom right: *The real part of the solution of the transmission problem with the incident wave consisting of both P- and S-components.*

The results of the wave propagation example (Section 6.1) suggest that the ratio of S- and P-wave basis functions s_k/p_k should be about the local ratio of the wave numbers κ_S/κ_P. By setting $s_k/p_k = \kappa_S/\kappa_P$, we compare two approaches for choosing the total element by element number of basis functions. The first, and the most obvious method, is to use an equal number of P-wave basis functions in all elements. Naturally, the total number of basis functions is then defined by the local ratio $s_k/p_k \approx \kappa_S/\kappa_P$. The second method is to choose the total number of basis functions for each element K_k so that the condition number of the corresponding matrix block D_k is below a user supplied allowed limit. More precisely, we use the highest number of P-wave basis functions which results in the condition number below this limit.

This approach is similar to that used in [13] for the ultra weak approximation of the Helmholtz problem. By varying the desired condition number we can vary the number of directions per element. Although only offering an indirect control over the accuracy of the solution, this pragmatic approach helps ensure that the iterative scheme converges. The mesh is fixed (Fig. 6.10) so we are essentially using the p-UWVF studied in Fig. 6.6. In particular the polygonal approximation of the circular scatterer does not improve with more degrees of freedom.

In this part of the study we use the material parameters listed for Ex. 1. in Table 6.3. Note that the inhomogeneity and the background materials have a remarkably different ratios c_P/c_S. Accordingly, the ratio s_k/p_k has the same variation between the two domains. The solution of the problem for (P+S)-wave incident field (i.e. $\alpha = 1$, $\beta = 1$ in (6.1)) and for $f = 1.0 \cdot 10^4$ is shown in Fig. 6.10.

The error and the maximum condition number of D_k as a function of the number of degrees of freedom (DOF) for, respectively, a fixed and a non-uniform distribution of the number of P-wave basis functions per element are shown in Fig. 6.11. In this figure, the relative error refers to the difference between the UWVF solution and the analytic Fourier series solution. We note that using a uniform distribution of the number of P-wave basis functions per element results in a rapid deterioration of the conditioning of the problem which causes a blow-up of the error. Therefore, in the remaining examples, the number of basis functions is chosen according to the conditioning of D_k as described above.

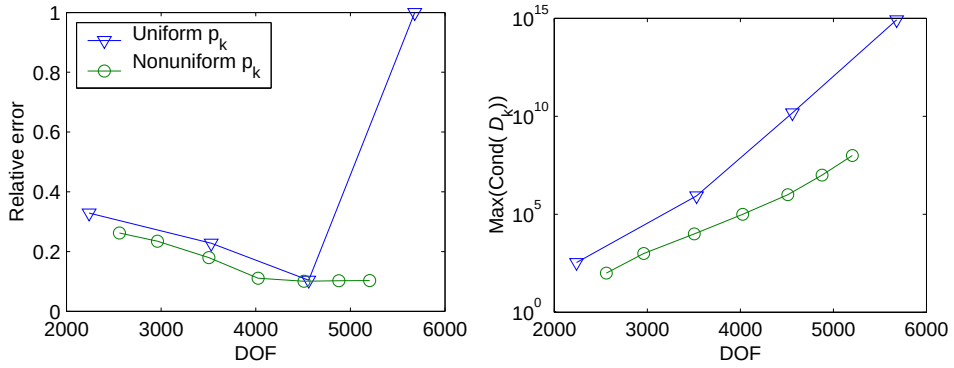

FIGURE 6.11. *Comparison of two approaches for choosing the total number of basis functions. The nonuniform number of P-wave basis functions p_k for the element K_k is chosen based on the condition number of the matrix block D_k. In both cases the number of S-wave basis functions is defined by the local ratio of wavenumbers as $s_k/p_k = \kappa_S/\kappa_P$.*

Although the wave propagation example indicates that the ratio of S- and P-wave basis functions should be about equal to the ratio of the S- and P-wavenumbers, it is worthwhile to confirm this hypothesis also for a more complex problem. As in the previous section, we study next the effect of the choice of the ratio s_k/p_k of the basis functions on the accuracy of the elastic UWVF approximation. To obtain an almost homogeneous ratio of the wave numbers in the whole computation domain, we use the material parameters of Ex. 2. from Table 6.3. The wavenumbers for the two subdomains are different, causing significant scattering of waves from the interface, but the ratio c_P/c_S is approximately equal for both materials. This allows a straightforward comparison between the ratios s_k/p_k and κ_S/κ_P; and performance of the UWVF.

Since the number of basis functions for each element is chosen now according to the condition number of D_k, we show the relative error as a function of the maximum allowed condition number in Fig. 6.12. The composition of the basis is varied by changing the ratio of S- and P-wave basis functions s_k/p_k. The results are computed for both P- and S-wave incident fields.

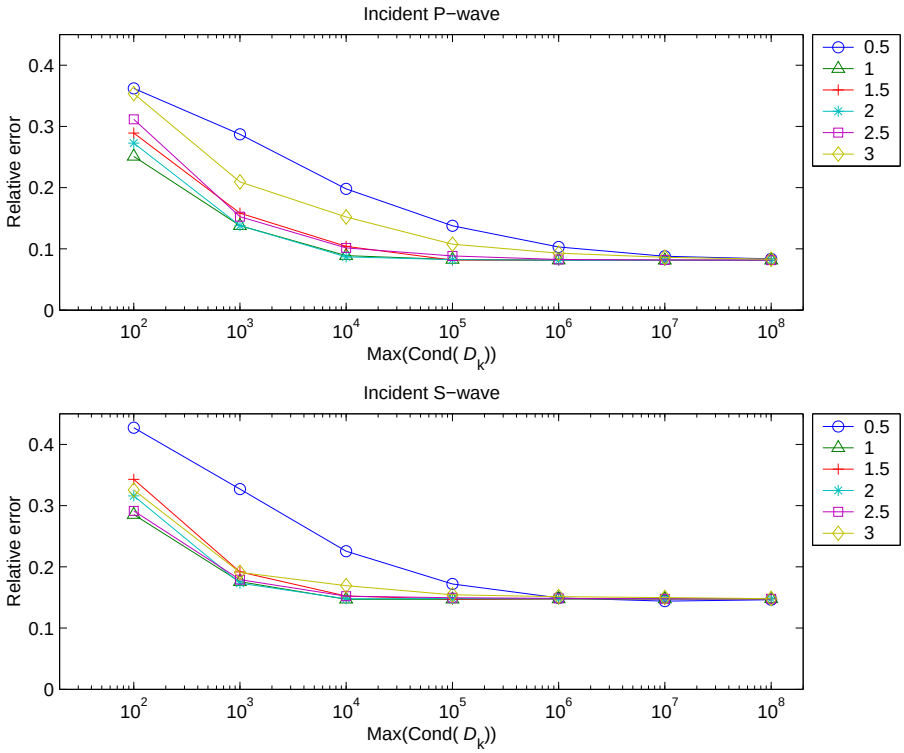

FIGURE 6.12. *Relative error as a function of maximum condition number of the blocks D_k. Each curve shows the error for a fixed ratio of s_k/p_k. The maximum accuracies for the incident P- and S-waves are 8% and 15% respectively. The discrepancy of this order between the Fourier series and UWVF approximations are due to low order absorbing boundary condition and the approximation of the curved boundary by the UWVF.*

The error for the same set of simulations is shown as a function of the number of degrees of freedom in Fig. 6.13. It is notable that the error in the solution can be controlled by choosing the desired maximum condition number (this in turn effects the convergence rate of the bi-conjugate gradient scheme which may not converge if the condition number is chosen too large). Of course the asymptotic error in the computed solution is different for S- and P-incident waves because of the differences in the scattered wave in each case.

7. Conclusions. We have formulated a discrete UWVF scheme for approximating the time harmonic elastic wave equation in two dimensions. The method obviously extends to three dimensions. This requires, however, an additional set of S-wave basis functions, since in three dimensions the elastic wave consists of the P-wave and two polarizations of S-waves known as horizontal (SH-) and vertical (SV-) waves. Based on our experience with the Helmholtz equation in two and three dimensions we expect the method to compare favorably to a low order finite element scheme (see [4] for work

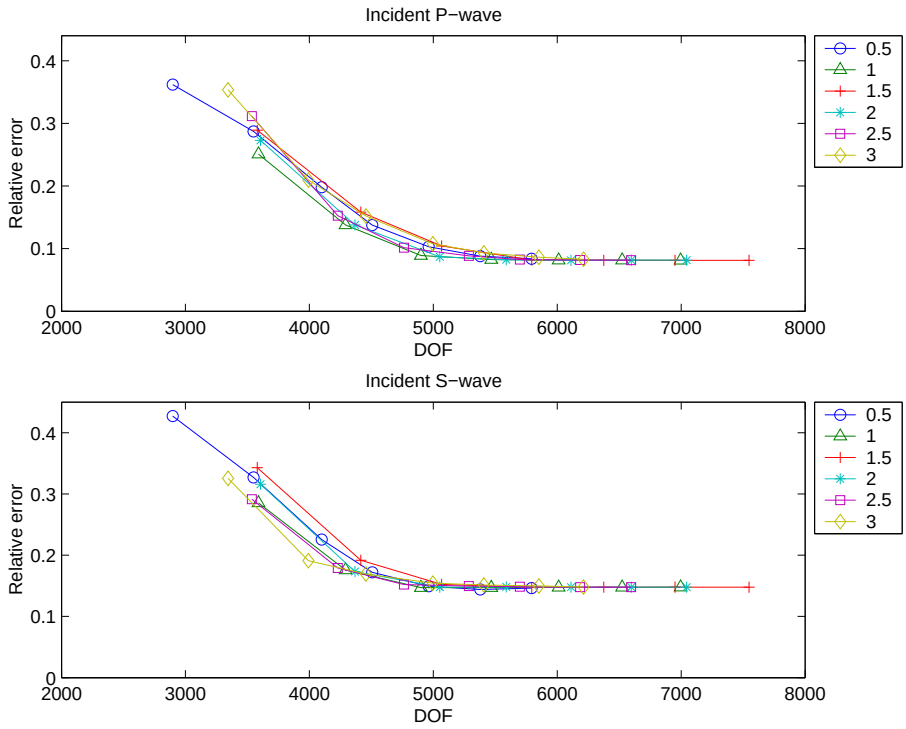

FIGURE 6.13. *Relative error as a function of the number of degrees of freedom.*

estimates).

Our numerical results in 2D show that the method can compare favorably to low order finite element methods, and that potential conditioning problems can be controlled by choosing the plane wave basis in the right way. Ultimately our goal, to be reported in a future publication, is to use the elastic UWVF together with acoustic-UWVF to obtain a high order coupled fluid-structures code.

The theoretical analysis of the elastic UWVF (and other UWVF methods) needs more work. The current analysis of the elastic UWVF only proves that a discrete solution exists, and we are working to provide an error analysis. Finally the elastic UWVF needs further testing on wide range of practical problems (incorporating, for example, edge effects) in order to more completely validate the method.

REFERENCES

[1] J.D. ACHENBACH *Quantitative nondestructive evaluation*, International Journal of Solids and Structures, 37 (2000), pp. 13-27.

[2] B.A. AULD, *Acoustic Waves and Fields in Solids, Vol. 2* , John Wiley and Sons,1973.

[3] I. BABUŠKA AND J.M. MELENK, *The partition of unity method*, International Journal for Numerical Methods in Engineering, **40** (1997), pp. 727-758.

[4] O. CESSENAT, *Application d'une nouvelle formulation variationelle aux équations d'ondes harmoniques. Problèmes de Helmholtz 2D et de Maxwell 3D*, Ph.D. Thesis, Paris IX Dauphine (1996)

[5] O. CESSENAT AND B. DESPRÉS, *Application of an ultra weak variational formulation of elliptic PDEs to the two-dimensional Helmholtz problem*, SIAM J. Numer. Anal., **35** (1998), pp. 255–299.

[6] O. Cessenat and B. Després, *Using plane waves as base functions for solving time harmonic equations with the ultra weak variational formulation*, Journal of Computational Acoustics, **11** (2003), pp. 227-238.
[7] D. Braess, *Finite Elements*, Cambridge University Press, 2001 (second edition).
[8] P.A. Gauzellino, J.E. Santos and D. Sheen, *Frequency domain wave propagation modeling in exploration seismology* , Journal of Computational Acoustics, **9** (2001) pp. 941-955
[9] E. Giladi and J.B. Keller, *A hybrid numerical asymptotic method for scattering problems*, J. Comput. Phys. **174** (2001), pp. 226-247
[10] K.F. Graff, *Wave Motion in Elastic Solids*, Dover Publications,1991.
[11] I. Harari and S. Haham, *Improved finite element methods for elastic waves*, Comput. Methods. Appl. Mech. Eng., **166** (1998), pp. 143-164
[12] R.L. Higdon, *Radiation boundary conditions for elastic wave propagation*, SIAM J. Numer. Anal.,**27** (1990), pp. 831–869.
[13] T. Huttunen, P. Monk, and J.P. Kaipio, *Computational aspects of the ultra weak variational formulation*, J. Comput. Phys., **182** (2002), pp. 27-46
[14] L. Halpern, *Etude de conditions aux limites absorbantes pour des schemas numeriques relatifs a des equations hyperboliques lineaires*, Ph.D. Thesis, Universite Paris VI, Place Jussieu, Paris, (1980).
[15] M. Hayner and K. Hynynen, *Numerical analysis of ultrasonic transmission and absorption of oblique plane waves trough the human skull* , J. Acoust. Soc. Amer. **110** (2001), pp. 3320-3330
[16] G.C. Hsiao, R.E Kleinman, and F.R Roach, *Weak solutions of fluid-solid interaction problems*, Math. Nachr., **218** (2000), pp. 139–163.
[17] V.D. Kupradze, *Potential Methods in the Theory of Elasticity*, Israel Program of Scientific Translations, 1965.
[18] F. Ihlenburg, *Finite Element Analysis of Acoustic Scattering*, Springer-Verlag, 1998.
[19] O. Laghrouche, P. Bettess and R.J. Astley, *Modeling of short wave diffraction problems using approximating systems of plane waves*, Int. J. Numer. Methods Eng., **54** (2002), pp. 1501-1533
[20] Y-H. Pao, and C-C. Mow , *Diffraction of Elastic Waves and Dynamic Stress Concentrations*, Crane-Russak Inc., New York, (1973)
[21] E. Perrey-Debain, J. Trevelyan and P. Bettess, *P-wave and S-wave decomposition in boundary integral equation for plane elastodynamics*, preprint (2002).
[22] E. Perrey-Debain, J. Trevelyan and P. Bettess, *Use of wave boundary elements to extend discrete methods in acoustics computations to higher frequencies*, Proceedings of WCCM-V, preprint (2002).
[23] J. Sun and K. Hynynen *Focusing of therapeutic ultrasound through a human skull: A numerical study*, J. Acoust. Soc. Amer. **104** (1998), pp. 1705-1715
[24] A. Quarterioni, A. Tagliani and E. Zampieri, *Generalized Galerkin approximations for elastic waves with absorbing boundary conditions*, Comput. Methods. Appl. Mech. Eng., **163** (1998), pp. 323–341.